Mechatronics 118 (2026) 103554

Contents lists available at ScienceDirect

Mechatronics

journal homepage: www.elsevier.com/locate/mechatronics

Robust reset control design by loop shaping for piezoelectric-actuated positioner in presence of nonlinearity☆,☆☆

A. Sebghati *, S.H. HosseinNia

Department of Precision and Microsystems Engineering, Faculty of Mechanical Engineering, Delft University of Technology, The Netherlands

ARTICLE INFO

Keywords:
High-performance motion control systems
Loop shaping
CgLp reset control
Shaping filter
Describing function
Piezo-actuated stage

ABSTRACT

Loop-shaping is widely used in precision motion control, but conventional approaches — focused on phase margin and open-loop gain — are inadequate for piezo positioning systems where open-loop phase critically affects performance. This paper proposes generalized loop-shaping guidelines tailored for nonlinear piezo-actuated stages. A constant-in-gain lead-in-phase reset controller is developed to implement the guidelines by overcoming waterbed effect in linear control. An intuitive methodology for shaping filter design is presented to ensure reliable reset control implementation. Using (higher-order) sinusoidal input describing functions, nonlinear motion control is designed. Experiments demonstrate closed-loop bandwidth flatness (±1 dB) and enhanced sensitivity function.

1. Introduction

Loop-shaping is a well-established frequency-domain methodology for linear control design, widely applied in precision motion systems to achieve high performance (precision and bandwidth) and stability margins, as reflected by the closed-loop and sensitivity functions. Traditionally, it focuses on the open-loop phase near the crossover frequency (the frequency where the open-loop gain crosses 0 dB) to ensure robust stability and desirable transient characteristics (characterized by phase-margin constraint), while performance is tuned via the crossover frequency and the open-loop gain shaping (see, e.g., [1]). Unfortunately, this traditional approach is not adequate for ultra-precision motion systems.

In piezo-actuated positioning systems with very high stiffness and lightly-damped resonance, the open-loop phase is also critical for performance where the open-loop gain unavoidably remains close to unity over a wide frequency range around the crossover frequency — the unity gain crisis not captured by conventional methods — due to performance-stability trade-offs. For piezoelectric nanopositioning stages, offering superior precision and bandwidth over electromagnetic actuators (see, e.g., [2]), a flatness of ±1 dB in the closed-loop response in addition to the maximum possible cross-over frequency is typically desired, which conventional loop-shaping struggles to achieve due to missing the open-loop phase shaping in the frequency range of crisis.

This work shows that shaping the open-loop phase over a wide frequency range — without altering the gain — can extend the crossover frequency while preserving the flatness constraint. However, such phase enhancement requires a constant-in-gain lead-in-phase (CgLp) filter, unavailable in linear control. Reset control, introduced by Clegg [3], serves as one of the control types (see, e.g., [4] for another type) that provides a nonlinear means to overcome this limitation (see, e.g., [5–7]). CgLp reset control closely approximates this property and has enabled high-performance motion control, thanks to the recently developed analytical frequency-domain tools (see, e.g., [8]). Although integration of a reset element leads to a nonlinear motion control (see, e.g., [9]), recent advancements have enabled reset control design by loop shaping. The phase advantage can be analyzed via the sinusoidal input describing function (SIDF), though higher-order SIDF (HOSIDF) analysis reveals limitations due to the generated higher-order harmonics in feedback characterized by multiple resets per cycle [10]. Shaping filters [11,12] can mitigate these effects, though generalized design guidelines remain lacking.

Nonlinearities in piezo actuators, such as hysteresis and amplifier saturation, further limit achievable performance in a large travel range (see, e.g., [13]). Feedforward compensation can reduce but not eliminate these effects [14,15]. Thus, there is a need to a robust motion control to preserve performance against the nonlinearities. Although measured frequency response generally represents linear dynamics, the

☆ This article is part of a Special issue entitled: 'TC 4.2 Mechatronic Systems (IFAC WC 2026)' published in Mechatronics.

☆☆ This work was financed by Physik Instrumente (PI) SE & Co. KG and co-financed by Holland High Tech with PPS Project supplement for research and development in the field of High Tech Systems and Materials.

* Corresponding author.
E-mail addresses: a.sebghati@tudelft.nl (A. Sebghati), s.h.hosseinniakani@tudelft.nl (S.H. HosseinNia).

https://doi.org/10.1016/j.mechatronics.2026.103554
Received 3 November 2025; Received in revised form 6 May 2026; Accepted 13 May 2026
Available online 2 June 2026

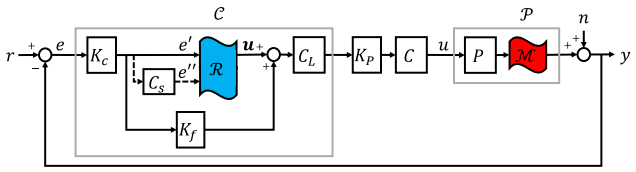

Fig. 1. Control loop elements; $\mathcal{P}$: Plant's uncertain dynamics, P: nominal measured frequency response, $\mathcal{M}$: Multiplicative uncertainty. C: Linear control. K_P: Proportional gain. $\mathcal{C}$: CgLp control, $\mathcal{R}$: First-order reset element, C_s: Shaping filter, k_c, k_f: CgLp internal parameters, C_L: Lead filter.

HOSIDF [16] provides a means to characterize such nonlinearities as frequency-domain uncertainties. However, the measurement-based use of the HOSIDF in piezo-actuated systems remains unexplored [17].

This paper integrates loop-shaping theory, practically effective reset control, and nonlinear analysis into a unified framework. The main contributions are:

- New loop-shaping guidelines enabling high cross-over frequency and flat closed-loop response (±1 dB) even if the open-loop gain is unavoidably near unity in a wide frequency range;
- Extension to uncertain systems ensuring robustness in performance;
- A CgLp reset controller with a generalized shaping-filter synthesis method for viable open-loop phase shaping;
- Use of HOSIDF to represent nonlinearities in piezo actuators as frequency-domain uncertainties by real measurements.

The paper is organized as follows: Section 2 gives the required mathematical tools. Section 3 describes the experimental setup and nonlinearity characterization. The problem is also motivated. Section 4 develops the analytical formulations for loop shaping; Section 5 details nonlinear control design; Section 6 reports experimental validation; and Section 7 concludes.

2. Preliminaries

The feedback control structure is considered as Fig. 1.

The piezo stage system is categorized by the uncertain dynamics $\mathcal{P}$ as follows:

$$\mathcal{P}(j\omega) = P(j\omega).\mathcal{M}(j\omega) \tag{1}$$

where P and $\mathcal{M}$ respectively denote the measured frequency response for small input's amplitude and the frequency-domain multiplicative uncertainty due to larger travel ranges. In this work, $\mathcal{M}$ is obtained by the ratio between P and the 1st-order sinusoidal input describing function, assuming that the amplitudes of the higher-order sinusoidal input describing functions are negligible. Therefore, $\mathcal{P}$ is represented by an uncertain region in the Bode plane that contains P.

$C(j\omega)$ stands for linear control elements with the unity DC gain. K_P is used to set the cross-over frequency ω_c. $\mathcal{C} = 1$ is selected to represent a scenario of linear motion control design; otherwise, $\mathcal{C}$ denotes the constant-in-gain lead-in-phase (CgLp) reset control for the scenario of the nonlinear motion control design.

The generalized first-order reset element $\mathcal{R}$ with the state–space dynamics below is used to construct the CgLp reset control:

$$\begin{cases} \dot{\boldsymbol{x}}(t) = -\omega_r' \boldsymbol{x}(t) + \omega_r' e' & \text{if } e''(t) \neq 0 \\ \boldsymbol{x}(t^+) = \gamma \boldsymbol{x}(t) & \text{if } e''(t) = 0 \\ \boldsymbol{u}(t) = \boldsymbol{x}(t) \end{cases} \tag{2}$$

where $e', \boldsymbol{x}, \boldsymbol{u} \in \mathbb{R}$ respectively denote the input, state and output of the reset element. e'' is produced by the shaping filter C_s that is used for the resetting condition. The shaping filter lets bandpass the control nonlinearity in the required frequency range (see, e.g., [11]).

The hybrid dynamics of the reset control consists of the base linear dynamics $\mathcal{R}_{\text{bl}}$ and the switching dynamics $\mathcal{R}_{\text{r}}$, represented by the first and the second differential equation in (2) respectively. $\omega_r' \in \mathbb{R}_{++}$ is the corner frequency of the base linear dynamics and $\gamma \in (-1, 1) \subset \mathbb{R}$ is the resetting coefficient of the switching dynamics.

The 1st-order and higher-order sinusoidal input describing functions $\mathcal{R}_1$ and $\mathcal{R}_n$ of generalized first-order reset element (2) are given by Guo et al. [18], Hou et al. [19], Zhang and HosseinNia [20] as follows:

$$\begin{aligned} &\mathcal{R}_1(j\omega) = \tfrac{1}{j\frac{\omega}{\omega_r'}+1}.(1 + j\Theta_N), \\ &\mathcal{R}_n(j\omega) = \begin{cases} \tfrac{1}{j\frac{n\omega}{\omega_r'}+1}.j\Theta_N e^{j(n-1)\angle C_s} & \text{if } n : \text{odd} \\ 0 & \text{if } n : \text{even}, \end{cases} \\ &\Theta_N = \hat{\Theta}.\Theta_s, \\ &\hat{\Theta} = \tfrac{2\omega(1-\gamma)(1+e^{-\pi\frac{\omega_r'}{\omega}})}{\pi(1+\gamma e^{-\pi\frac{\omega_r'}{\omega}})(\omega^2+\omega_r'^2)}, \\ &\Theta_s = e^{j\angle C_s}(\omega\cos(\angle C_s) + \omega_r' \sin(\angle C_s)) \end{aligned} \tag{3}$$

Fig. 2(a) visualizes the phase advantage of reset element (2) with no shaping filter ($C_s = 1$) compared to its base-linear dynamics. The phase lag reduces as γ decreases from 1 (base-linear dynamics) to -1 with negligible change in gain according to the 1st-order describing function—implying that the Bode's gain-phase relationship which is the inherent limitation of linear control elements is flexed in the reset element. This phase advantage highlights an opportunity for approximating a constant-in-gain lead-in-phase dynamics by $\mathcal{C}$.

The first-harmonic frequency response of the nonlinear control is denoted by $\mathcal{C}_1$ and calculated by

$$\mathcal{C}_1(j\omega) = k_c.(\mathcal{R}_1(j\omega) + k_f).C_L(j\omega) \tag{4}$$

where the lead filter C_L together with the proportional gains k_c, k_f are selected as follows such that the frequency response characteristics of $\mathcal{C}_1$ is CgLp [21]:

$$\begin{aligned} &C_L(j\omega) = \tfrac{j\frac{\omega}{\omega_r}+1}{j\frac{\omega}{\omega_f}+1}, \\ &\omega_r = \alpha\omega_r', \alpha = \sqrt{1 + \tfrac{16}{\pi^2}(\tfrac{1-\gamma}{1+\gamma})^2}, \\ &k_f = \tfrac{\omega_r}{\omega_f - \omega_r}, k_c = 1 - \tfrac{\omega_r}{\omega_f} \end{aligned} \tag{5}$$

Fig. 2(b) visualizes $\mathcal{C}_1$ for different γ. Such a property is not realizable by linear control (for example, an effort will end up to the unstable dynamics with transfer function $\frac{s+\omega_r}{s-\omega_r}$).

On the other hand, the phase advantage from reset control is entangled with the cost of higher-order harmonics. To utilize reset control in feedback, the following two assumptions are considered [8]:

- The reset element output and thus the closed-loop response are input-to-state convergent.
- Resetting time instants occur periodically with the time interval similar to a single sinusoid with the first harmonic.

The convergence in the earlier assumption has been studied by Dastjerdi et al. [22] where investigation of closed-loop stability and H_β-condition [23–28] are extended to the frequency domain for the primary versions of CgLp reset control. Performance is validated by the frequency-domain tools which will be provided later in this section. For a reliable control design based on the 1st-order describing function, zero-crossing more than two times per cycle, which is referred to as multiple reset, is not permitted with regard to the latter assumption. Shaping filter allows for tuning the phase advantage alongside frequency as a trade-off technique with the higher-order harmonics to ensure a reliable feedback control design. Shaping filter will be further discussed in Section 5.1.

For the case of the linear motion control, where $\mathcal{C} = 1$, the sensitivity and complementary sensitivity functions S and T are given

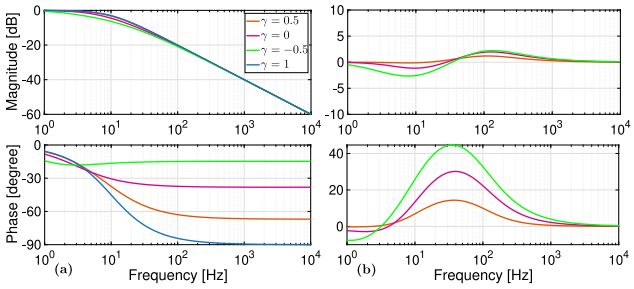

Fig. 2. Frequency response characteristic of reset control based on sinusoidal input describing function; (a) Generalized first-order reset element with $\omega_r = 2\pi \times 10$ rad/s. (b) Constant-in-gain lead-in-phase realization with $\omega_r = 2\pi \times 10$ rad/s, $\omega_f = 2\pi \times 100$ rad/s.

by

$$S(j\omega) = \frac{1}{1+L(j\omega)}, T(j\omega) = \frac{L(j\omega)}{1+L(j\omega)}, \\ L(j\omega) = K_P.C(j\omega).\mathcal{P}(j\omega) \tag{6}$$

where L denotes the open-loop function. In the case of the nonlinear motion control, higher-order harmonics are generated due to the reset control. In this case, it is first assumed that the higher-order harmonics have negligible effects on the performance during the control design process. Therefore, sensitivity and complementary sensitivity functions $\mathcal{S}_1$ and $\mathcal{T}_1$ below are considered for control design [8]:

$$\mathcal{S}_1(j\omega) = \frac{1}{1+\mathcal{L}_1(j\omega)}, \mathcal{T}_1(j\omega) = \frac{\mathcal{L}_1(j\omega)}{1+\mathcal{L}_1(j\omega)}, \\ \mathcal{L}_1(j\omega) = C_1(j\omega).K_P.C(j\omega).\mathcal{P}(j\omega) \tag{7}$$

where $\mathcal{L}_1$ denotes the open-loop function based on the 1st-order describing function. Next, the frequency-domain tools pseudo-sensitivity and pseudo-complementary sensitivity functions S_∞ and T_∞ below are used to validate the control design based on the 1st-order describing function regarding the higher-order harmonics [8]:

$$S_\infty(j\omega) = \max\{\Sigma_{i=1}^{\infty}|\mathcal{S}_i(j\omega,\kappa)|\sin(n\omega t + \measuredangle\mathcal{S}_i(j\omega,\kappa))\}, \\ \mathcal{T}_\infty(j\omega) = \max\{\Sigma_{i=1}^{\infty}|\mathcal{T}_i(j\omega,\kappa)|\sin(n\omega t + \measuredangle\mathcal{T}_i(j\omega,\kappa))\} \tag{8}$$

$\mathcal{S}_n$ and $\mathcal{T}_n$ capture the higher-order harmonics effects that are calculated by:

$$\mathcal{S}_n(j\omega) = -\mathcal{T}_n(j\omega) = -S_{bl}(jn\omega).\mathcal{L}_n(j\omega). \\ \frac{(S_1(j\omega))^n}{|S_1(j\omega)|^{n-1}}.\frac{(R(j\omega))^{n-1}}{|R(j\omega)|^{n-1}}, S_{bl}(j\omega) = \frac{1}{1+L_{bl}(j\omega)}, \\ L_{bl}(j\omega) = C_{bl}(j\omega).K_P.C(j\omega).\mathcal{P}(j\omega), C_{bl}(j\omega) = \\ \mathcal{R}_{bl}(j\omega).C_L(j\omega), \mathcal{L}_n(j\omega) = C_n(j\omega).K_P.C(jn\omega). \\ \mathcal{P}(jn\omega) \tag{9}$$

The subscript *bl* refers to the base linear dynamics of the associated element. R denotes the complex coefficient of the sinusoidal reference in the Fourier series. S_∞ and T_∞ are representative of the all harmonics effects that must be close to S_1 and T_1 for the performance to be preserved against the higher-order harmonics.

The open-loop bandwidth is defined by the frequency range $(0, \omega_c]$. The cross-over frequency ω_c is the angular frequency at which $|L|$ or $|\mathcal{L}|$ crosses 0 dB. The closed-loop bandwidth is categorized by the maximum frequency up to which the complementary sensitivity function $|T|$ or $|\mathcal{T}|$ is close to the 0 dB line. A hard metric for the closeness is defined by the ±1 dB bound around the 0 dB in case of the piezo-actuated stages.

3. Problem statement

3.1. Nano-positioning system

A piezoelectric-actuated nano-positioning stage of the type P-621.1CD PIHera is considered as a case study to motivate the problem and validate the developed control scheme by experiments. The plant is equipped with a stack piezoelectric as the actuator with the maximum open-loop travel range of the $[-10, 120]$ μm. A photo of the laboratory setup is given in Fig. 3.

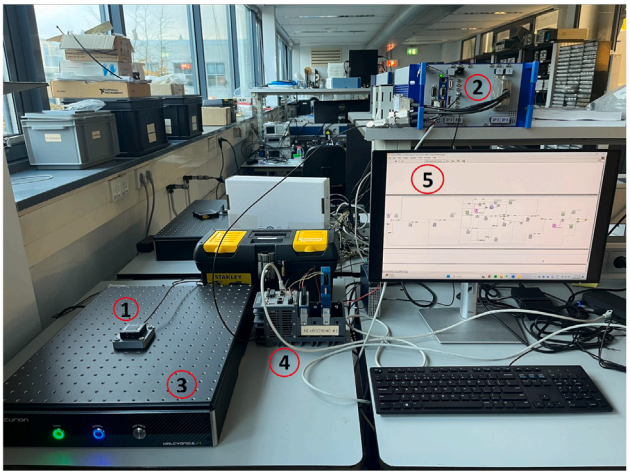

Fig. 3. Laboratory setup: (1) Piezoelectric stage with capacitor sensor, (2) E712 module, (3) Vibration isolation table, (4) CompactRio/FPGA, (5) Host personal computer.

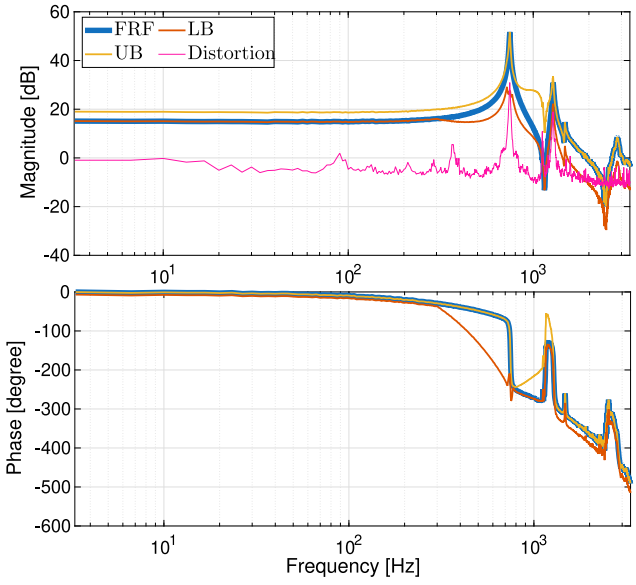

Fig. 4. Plant dynamics: The nominal frequency response function (FRF) and the total distortion based on the multi-sine identification. The lower bound (LB) and the upper bound (UB) on uncertain FRF.

The linear dynamics of the plant is identified by the measured frequency response as in Fig. 4. There is a lightly-damped resonance at high frequency where phase lag due to delay is significant. The resonance is closely followed by a high mode.

A multi-sine input voltage equivalent to a travel range of 1 μm is used to identify the linear dynamics around the position 50μm. The distortion thus represents the standard of deviation due to noise and nonlinearity. It is concluded that the nominal frequency response function is reliable around the selected operating point for sufficiently small input amplitudes.

Fig. 5 depicts the measured 1st-harmonic and 2nd-harmonic sinusoidal input describing function of the plant for different travel ranges. The maximum amplitude of the 2nd harmonic is much below the

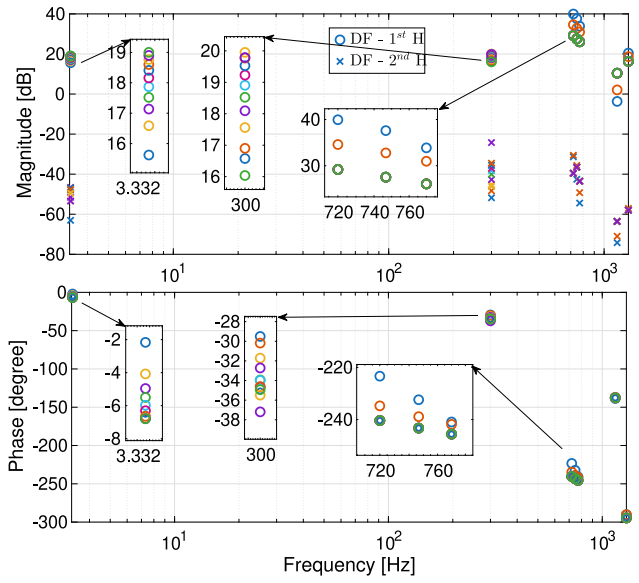

Fig. 5. 1st-order and 2nd-order describing function measurements at frequencies {3.3,300,720,747,770,1150,1297} Hz for input voltages {0.25,0.5,1,1.5,2,2.5,3,3.5,4,4.5,5,5.5} V at low frequency. The input voltages {0.25,0.5,1} V are selected around the resonances and anti-resonances since there will be (anti)notch filters in the control loop.

minimum amplitude of the 1st harmonic. The results leave a fair assumption that the travel range, or the nonlinearity, mostly appears as a variation in the 1st-order describing function. Therefore, an appropriate nonlinear model for the plant in the frequency-domain is given by the uncertain region on top of the nominal frequency response as depicted in Fig. 4.

3.2. Motivation

The aim for piezoelectric-based nano-technology is to achieve ultra-high precision and closed-loop bandwidth in positioning beyond the capability of the other precision motion systems e.g., electromagnetic actuators. In some applications, e.g., scanning, the real position is needed to precisely track high-speed references with the precision of ± 1 dB in magnification−a phase shift between the reference and the real position is not important and it can be compensated by time-advancing the reference. As there have been difficulties in implementing feed-forward control for piezo systems due to system's nonlinearities, this time-domain performance metric is mainly reflected by the magnitude of the complementary sensitivity function $|T|$. Therefore, the following frequency-domain constraint is required to hold in the closed-loop bandwidth while pushing the closed-loop bandwidth frequency forward:

$$\text{Constraint: } |T(j\omega)| \in [-1, +1] \text{ dB} \tag{10}$$

Rejection of disturbances and uncertainties defines the other important aspect of precision, which is captured by the peak of error e in Fig. 1. This time-domain performance metric is reflected by the magnitude of the sensitivity function $|S|$. For piezo systems, the following frequency-domain objective function is thus required to hold with an aim for the precision of nano-meter level in positioning:

$$\text{Objective function: minimize } |S(j\omega)| \tag{11}$$

Loop shaping is a standard methodology to optimize linear motion control for precision systems in industry.

Based on the traditional guidelines by loop shaping, performance and robust stability are often optimized by a high cross-over frequency ω_c, high and low open-loop gain $|L|$ respectively below and above ω_c, and a certain range of phase margin within a narrow neighbor around ω_c. The latter implies that $\angle L$ is paid attention only for robust stability. The traditional guidelines have shortcomings to fulfill requirements (10) and (11).

Table 1
The values of the control parameters.

Parameter	Value	Unit	Parameter	Value	Unit
ω_i	$2\pi \times 100$	rad/s	ω_i'	$2\pi \times 100$	rad/s
ω_m	$2\pi \times 747$	rad/s	ω_m'	$2\pi \times 1287$	rad/s
Q_1	50		Q_1'	5	
Q_2	0.5		Q_2'	0.5	
ω_c	$2\pi \times 200$	rad/s			
ω_r	$2\pi \times 10$	rad/s	ω_f	$2\pi \times 35$	rad/s
γ	−0.2		ω_h	$2\pi \times 500$	rad/s
ω_N	$2\pi \times 40$	rad/s	ω_A	$2\pi \times 410$	rad/s
Q_N	5		Q_A	0.05	
Q_N'	0.5		Q_A'	5	

To fulfill flatness requirement (10) with a high closed-loop bandwidth, the following open-loop gain property in addition to pushing the cross-over frequency f_c forward is needed according to the loop-shaping guidelines:

$$|L| \notin [-5.54, 19.28] \text{ dB} \tag{12}$$

Inequality (12) is derived from the second equation in (6). (10) is satisfied for an open-loop gain beyond 19.28 dB irrespective of the open-loop phase. Below −5.54 dB, $|T|$ is kept below the flatness region irrespective of the phase, which is desired above the bandwidth frequency. (12) implies that the slope of $|L|$ must be extremely high at ω_c. This is also needed to satisfy (11), and additionally $|L|$ must be as high as possible in the open-loop bandwidth. However, $|L|$ unavoidably remains close to the unity gain within a wide frequency range $\mathbb{F} = [F_1, F_2]$ around f_c, highlighting the particular challenge in systems such as piezo-stack actuators where the first resonance is lightly damped at very high frequency. This is in contrast to the requirement for the extremely high slope gain property, which is referred to as the unity gain crisis. The following example will illustrate why the frequency range of crisis $\mathbb{F}$ is created for a piezo-stack actuator.

Motivating example

The linear control below is applied to the nominal frequency response of the piezo system in Fig. 4:

$$\begin{aligned} C(j\omega) &= C_{PI}(j\omega).C_N(j\omega), \\ C_{PI}(j\omega) &= (1 + \tfrac{\omega_i}{j\omega}).(1 + \tfrac{\omega_i'}{j\omega}), \\ C_N(j\omega) &= \frac{(\frac{j\omega}{\omega_m})^2 + \frac{1}{Q_1\omega_m}.j\omega + 1}{(\frac{j\omega}{\omega_m})^2 + \frac{1}{Q_2\omega_m}.j\omega + 1} \cdot \frac{(\frac{j\omega}{\omega_m'})^2 + \frac{1}{Q_1'\omega_m'}.j\omega + 1}{(\frac{j\omega}{\omega_m'})^2 + \frac{1}{Q_2'\omega_m'}.j\omega + 1} \end{aligned} \tag{13}$$

A minimum set of linear elements have been selected. Two integrators with the corner frequencies ω_i, ω_i' are included to provide high $|L|$ in the open-loop bandwidth. Two notch filters with the corner frequencies ω_m, ω_m' are included to suppress the first two resonances for the stability and vibration considerations. The control parameters are selected as in Table 1 regarding the trade-off between high performance and high stability margins. K_P is selected such that the cross-over frequency ω_c is set to 200 Hz, which leaves a phase margin of 61°.

Fig. 6 depicts the shaped open-loop function L based on the traditional loop-shaping guideline and the consequence on the sensitivity and complementary sensitivity functions S, T. Fig. 6(a) shows the gain and phase of the open-loop function. In addition to the phase lag from delay, the notch filters distribute the resonances' phase lag till lower frequencies. Therefore, The integrations' cut-off frequencies ω, ω' have to be selected far below the first resonance to preserve robust stability−defined by a phase margin around $60° - 70°$. As a result, $|L|$ remains close to the stiffness line within a wide frequency range below

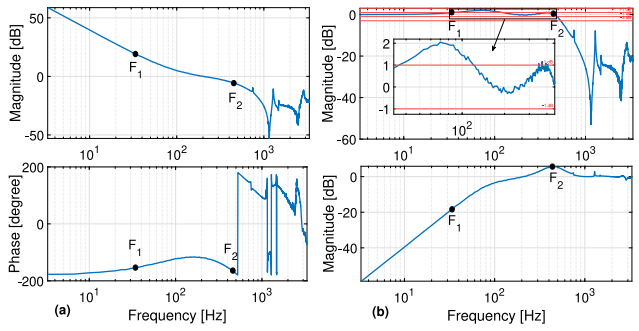

Fig. 6. Linear motion control; (a) Open-loop function, (b) Closed-loop and sensitivity functions. The critical frequency range $\mathbb{F}$ is indicated by the black circles.

the resonance frequency. Moreover, ω_c is restricted by this region to have a minimum phase margin. Therefore, the unity gain crisis is created within the critical frequency range $\mathbb{F} = [33, 443]$ Hz. From Fig. 6(b), two overshoots below and above the cross-over frequency ω_c are visible in the complementary sensitivity function, which implies that ± 1 constraint (10) is violated. Also, a concavity on the sensitivity function around 80 Hz is observed, which is not desired due to objective function (11).

It is noted that pushing ω_c forward by using the phase lead from a differentiation is not beneficial as it makes $\mathbb{F}$ wider. Therefore, the unity gain crisis becomes worse. Moreover, differentiation at high frequencies is avoided due to noise amplification.

In next section, the key role of the open-loop function's phase $\angle L$ in the closed-loop performance (10) and (11) in the critical frequency range $\mathbb{F}$ will be shown while $\angle L$ has been often paid attention only at the cross-over frequency ω_c. The developed theories are tailored to preserve robustness in performance against dynamics uncertainties. To utilize the theories, a constant-in-gain lead-in-phase (CgLp) element is needed to shape $\angle L$. Given that there is no linear element with a CgLp property, a new systematic methodology for shaping filter design is provided to let utilize CgLp reset control for this purpose.

4. New guideline in loop shaping

In the previous section, it was motivated that shaping the open-loop function gain $|L|$ is not sufficient for high-stiff motion systems with a lightly damped resonance, e.g., piezo-stack stage, to fulfill hard flatness constraint (10) and to prevent the creation of concavities on the magnitude of the sensitivity function in a wide frequency range $\mathbb{F}$. In this section, two analytical formulations are presented by two theories for systems with deterministic and uncertain frequency response functions respectively. The formulations determine the admissible region for the open-loop function phase $\angle L$ to let flatness constraint (10) hold in $\mathbb{F}$. The theories are followed by a remark to utilize the formulations such that the sensitivity function improves in $\mathbb{F}$. Consequently, new guideline for loop shaping is presented, revealing that the flatness constraint on $|T|$ is always achievable by shaping $\angle L$ in addition to $|L|$ as long as the dynamics uncertainties are limited. The new loop-shaping guideline is used to design the nonlinear control C in the next section.

Theorem 1. *Let the control structure be given by Fig. 1 with $\mathcal{M} = 1$ and $C = 1$. Furthermore, let the open-loop function, denoted by L, be represented by $\rho e^{j\theta}$ where $\rho \in \mathbb{R}_{++}, \theta \in \mathbb{R}$. For a given ρ, the open-loop phase requirement θ^* to achieve $|T| = p$ where $p \in \mathbb{R}$ is constant, is obtained by:*

$$\begin{aligned} &\theta^* = \arccos(D), \\ &D = -0.5\tfrac{1}{\rho} - 0.5\rho(\tfrac{p^2-1}{p^2}) \end{aligned} \tag{14}$$

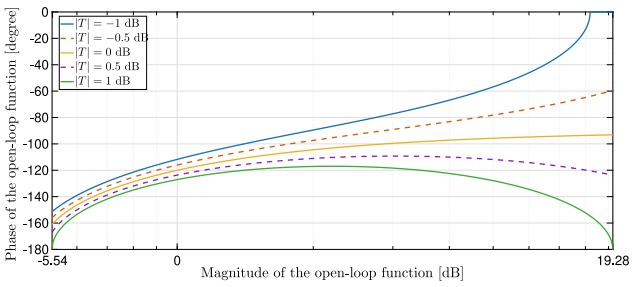

Fig. 7. Visualization of analytical formulation (14) in Theorem 1 and boundaries (17) in Corollary 2 for the ± 1 dB criterion.

and it is feasible if the following condition holds:

$$D \in [-1, 1] \tag{15}$$

Proof. The desired open-loop L^* is defined by $L^* := \rho e^{j\theta^*}$ and the additional phase requirement $\hat{\theta}$ is thus given by $\hat{\theta} = \theta^* - \theta$. The Cartesian representation $L = L_r + jL_i$ is considered. The equality constraint $|T| = p$ is therefore expanded as follows using (6):

$$\begin{aligned} &\tfrac{|L^*|}{|1+L^*|} = p \Rightarrow \tfrac{\rho}{|1+Le^{j\hat{\theta}}|} = p \Rightarrow \\ &\rho = p.|1 + (L_r + jL_i)(\cos\hat{\theta} + j\sin\hat{\theta})| \Rightarrow \\ &\sqrt{L_r^2 + L_i^2} = \\ &p.\sqrt{1 + 2L_r\cos\hat{\theta} - 2L_i\sin\hat{\theta} + L_r^2 + L_i^2} \Rightarrow \\ &1 + \tfrac{p^2-1}{p^2}\rho^2 = 2L_i\sin\hat{\theta} - 2L_r\cos\hat{\theta} = \\ &2L_r(\tfrac{L_i}{L_r}\sin\hat{\theta} - \cos\hat{\theta}) = 2L_r(\tfrac{\sin\theta}{\cos\theta}\sin\hat{\theta} - \cos\hat{\theta}) = \\ &2\tfrac{L_r}{\cos\theta}(\sin\theta\sin\hat{\theta} - \cos\theta\cos\hat{\theta}) = -2\rho\cos(\theta + \hat{\theta}) \\ &\Rightarrow \cos\theta^* = -0.5\tfrac{1}{\rho} - 0.5\rho.(\tfrac{p^2-1}{p^2}) \end{aligned} \tag{16}$$

If the pair of ρ, p are given such that the right side of the last equation belongs to $[-1, 1]$, analytical formulation (14) is derived by taking arccos from both sides of the last equation in (16). □

Corollary 2. *Following Theorem 1, the open-loop phase requirement θ^* is obtained as $\theta^* \in [\theta_m^*, \theta_M^*]$ to achieve $|T| = p$ where $p \in [p_m, p_M]$ unlike Theorem 1. The boundaries θ_m^*, θ_M^* are obtained by:*

$$\theta_m^* = \arccos(-0.5\frac{1}{\rho} - 0.5\rho.(\frac{p_M^2 - 1}{p_M^2})) \tag{17a}$$

$$\theta_M^* = \arccos(-0.5\frac{1}{\rho} - 0.5\rho.(\frac{p_m^2 - 1}{p_m^2})) \tag{17b}$$

and they are feasible if (15) respectively holds for $p = p_m, p_M$.

Proof. Analytical formulation (14) is decreasing with p. □

Fig. 7 visualizes derived analytical formulation (14) in Theorem 1 for different values of p and derived formulation (17) in Corollary 2 for $p \in [-1, 1]$. The solid curves determine the desired range of $\angle L$ for different values of $|L|$ which does not satisfy (12) if the flatness constraint on $|T|$ is considered as (10) with the ± 1 dB bound. The curves are plotted for the case that (12) does not hold and shaping $\angle L$ can satisfy the flatness constraint.

Next, a corollary is presented to let utilize Corollary 2 in the motion control design for a system with a deterministic dynamics.

Corollary 3. *Following Theorem 1 and Corollary 2, the required open-loop phase modification $\hat{\theta}$ for the system with the deterministic frequency response $P(j\omega)$ at each frequency ω is calculated by*

$$\hat{\theta}(\omega) = \theta^*(\omega) - \theta(\omega) \tag{18}$$

where θ^* is obtained by (17) and θ denotes the open-loop phase $\angle L$ for the given linear control C and K_P.

Proof. Following the proof of Theorem 1, $L(\omega) = \rho(\omega)e^{j\theta(\omega)}$ and $L^*(\omega) = \rho(\omega)e^{j\theta^*(\omega)}$. Analytical formulation (17) is applied at each frequency. □

In the following, the theories are extended to a system with an uncertain frequency response which is reflected by $\mathcal{M} \neq 1$.

Theorem 4. *Let the control structure be given by Fig. 1 with $\mathcal{M} = \eta e^{j\delta}$ and $C = 1$. The dynamics uncertainty is bounded in gain and phase as $\eta \in [\underline{\eta}, \overline{\eta}]$ with $\underline{\eta} \in (0, 1] \subset \mathbb{R}, \overline{\eta} \in [1, \infty) \subset \mathbb{R}$ and $\delta \in [\underline{\delta}, \overline{\delta}]$ with $\underline{\delta} \in (-\infty, 0] \subset \mathbb{R}, \overline{\delta} \in [0, \infty) \subset \mathbb{R}$. Furthermore, let the open-loop function, denoted by L, be represented by $\varrho e^{j\vartheta}$ where $\varrho \in \mathbb{R}_{++}, \vartheta \in \mathbb{R}$. The conserved open-loop phase requirement ϑ^* is obtained as $\vartheta^* \in [\vartheta^*_m, \vartheta^*_M]$ to robustly achieve $|T| = p$ where $p \in [p_m, p_M]$. The boundaries $\vartheta^*_m, \vartheta^*_M$ are obtained by:*

$$\vartheta^* \in [\vartheta^*_m, \vartheta^*_M] \tag{19a}$$

$$\vartheta^*_m = \boldsymbol{\vartheta^*_m} - \underline{\delta}, \vartheta^*_M = \boldsymbol{\vartheta^*_M} - \overline{\delta} \tag{19b}$$

$$\begin{aligned} &\boldsymbol{\vartheta^*_m} = \arccos\left(-0.5\tfrac{1}{\varrho} - 0.5\varrho.\left(\tfrac{p_M^2-1}{p_M^2}\right)\right), \\ &\varrho = \max\left(\min\left(\tfrac{p_M}{\sqrt{p_M^2-1}}, \overline{\varrho}\right), \underline{\varrho}\right), \underline{\varrho} = \rho.\underline{\eta}, \overline{\varrho} = \rho.\overline{\eta} \end{aligned} \tag{19c}$$

$$\boldsymbol{\vartheta^*_M} = \arccos\left(-0.5\tfrac{1}{\underline{\varrho}} - 0.5\underline{\varrho}.\left(\tfrac{p_m^2-1}{p_m^2}\right)\right) \tag{19d}$$

Proof. Following the proofs of Theorem 1 and Corollary 2, a robust region for the open-loop phase is needed with the robustness against $\mathcal{M}$. The proof continues for two cases as follows:

Case (A) $0 < p \leq 1$: The upper bound θ^*_M is increasing with ρ. Therefore, the solution of the relevant min–max optimization problem returns $\underline{\varrho} = \rho.\underline{\eta}$ to conserve θ^*_M as $\boldsymbol{\vartheta^*_M}$ against the gain uncertainty η. $\boldsymbol{\vartheta^*_M}$ is further conserved as ϑ^*_M against the phase uncertainty δ.

Case (B) $p > 1$: The Hessian of the lower bound θ^*_m with respect to ρ is negative and its local minimum exists at $\rho = \frac{p_M}{\sqrt{p_M^2-1}}$. Therefore, the solution of the relevant max–min optimization problem returns $\boldsymbol{\varrho}$ to conserve θ^*_m as $\boldsymbol{\vartheta^*_m}$ against η. $\boldsymbol{\vartheta^*_m}$ is further conserved as ϑ^*_m against δ. □

Fig. 8 visualizes derived analytical formulation (19) in Theorem 4 for a specific uncertainty bound. It is shown how the nominal region in Fig. 7 shrinks to the robust region for the open-loop phase requirement.

Next, a corollary is presented to let utilize Theorem 4 in the motion control design for a system with bounded dynamics uncertainty.

Corollary 5. *Following Theorem 4, the required open-loop phase modification $\hat{\vartheta}$ for the system with the uncertain frequency response $\mathcal{P}(j\omega)$ at each frequency ω is calculated by*

$$\hat{\vartheta}(\omega) = \vartheta^*(\omega) - \theta(\omega) \tag{20}$$

where ϑ^* is obtained by (19) and θ denotes the open-loop phase $\angle L$ for the given linear control C and K_P.

Proof. Following the proof of Theorem 1, $L(\omega) = \varrho(\omega)e^{j\vartheta(\omega)}$ and $L^*(\omega) = \varrho(\omega)e^{j\vartheta^*(\omega)}$. Analytical formulation (19) is applied at each frequency. □

Remark 6. As a result of the robust region in Theorem 4 compared to the nominal region in Corollary 2, flatness constraint (10) becomes conservative as the following:

$$\begin{aligned} &\text{Conserved constraint: } |T(j\omega)| \in \mathbf{T}(j\omega), \\ &\mathbf{T}(j\omega) = [\underline{T}(j\omega), \overline{T}(j\omega)] \subset [-1, +1] \text{ dB} \end{aligned} \tag{21}$$

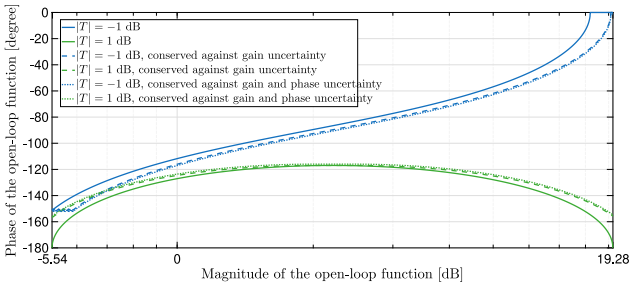

Fig. 8. Visualization of the conserved boundaries in Theorem 1 where $\underline{\eta} = 0.9, \overline{\eta} = 1.1, \underline{\delta} = \overline{\delta} = 1°$.

such that the complementary sensitivity function fulfills (10) in the worst cases of η and δ.

Next, two remarks are given to include sensitivity function improvement in shaping $\angle L$.

Remark 7. Constraints (10) and (21) are mapped onto the sensitivity function plane by (6) as lower and upper bounds that are respectively the nominal and conserved regions as the following:

$$\begin{aligned} &\text{Nominal bounds: } |S(j\omega)| \in \mathbf{S}^{\pm 1}(j\omega), \\ &\mathbf{S}^{\pm 1}(j\omega) = [\underline{S}^{\pm 1}(j\omega), \overline{S}^{\pm 1}(j\omega)] \text{ dB} \end{aligned} \tag{22a}$$

$$\begin{aligned} &\text{Conserved bounds: } |S(j\omega)| \in \mathbf{S}(j\omega), \\ &\mathbf{S}(j\omega) = [\underline{S}(j\omega), \overline{S}(j\omega)] \subset \mathbf{S}^{\pm 1} \end{aligned} \tag{22b}$$

The conserved region is then enlarged to $\boldsymbol{S}^{\pm 1}(j\omega)$ as the lower and upper bounds for the worst cases of η and δ. The bounds for the worst cases without shaping the open-loop function phase is denoted by the region $\boldsymbol{S}^{\pm 1}(j\omega)$.

Remark 8. The open-loop phase $\angle L$ plays a key role in the magnitude of the sensitivity function within the frequency range of crisis $\mathbb{F}$ since $|L|$ is close to 0 dB in this region. Based on (6) and (7), any phase lead in L reduces $|S|$ and vice versa. Therefore, Corollaries 3 and 5 are utilized such that any lag in phase is avoided.

The new guideline in loop shaping for the motion control design are therefore given as follows:

1. Increase the open-loop gain in the open-loop bandwidth (for example by integration) and increase the cross-over frequency ω_c.
2. For the deterministic case, $\mathcal{M} = 1$, go to step 3 and skip step 4. For the uncertain case, $\mathcal{M} \neq 1$, skip step 3 and go to step 4.
3. Apply Corollary 3 with regard to Remark 8 in the critical frequency range $\mathbb{F}$ to obtain the required range of the additional phase in the open-loop function L.
4. Apply Theorem 4 with regard to Remark 8 in the critical frequency range $\mathbb{F}$ to obtain the required range of the additional phase in L.
5. Realize the required modification in $\angle L$ by designing C.
6. Repeat steps 1 to 5 as long as C is feasible.

Based on the new loop-shaping guideline, C needs to provide phase lead without changing the gain ($|C| = 1$). There is no linear element with a constant-in-gain lead-in-phase (CgLp) property due to the Bode's gain phase relationship–the inherent limitation of linear control. In the next section, CgLp reset control is utilized, which enables the applicability of the new loop-shaping guideline in the motion control design. A systematic methodology for shaping filter design is presented to secure the reliability of the reset control design based on describing function.

5. Nonlinear motion control design

In this section, the motion control is designed for the piezo stage with the uncertain frequency response $\mathcal{P}$ as in Fig. 4 based on the new loop-shaping guideline given in the previous section. The actuator is supposed to operate in 25% of its full travel range around the operating point of 50 μm. Thus, the uncertain region of the system's dynamics is assumed to shrink by 25%. To design the motion control, the motivating example in Section 3.2 is considered. Nonlinear control will be included in the motion control to shape the open-loop phase based on Theorem 4. Therefore, it is expected to meet the performance metrics—the fulfillment of flatness constraint (10), which was violated by linear control even for the deterministic dynamics, and the improvement of sensitivity function by guarantee—while keeping the cross-over frequency ω_c the same as before. Step 6 of the given guideline is avoided to focus on the efficacy of the theorem and the validation of the control design.

Fig. 9 shows the nominal and robust regions to shape the phase of the open-loop function in the critical frequency range $\mathbb{F}$. The nominal regions are obtained by Corollaries 2 and 3 and the robust regions are obtained by Theorem 4 and Corollary 5. $\mathbb{F}' = [F_1', F_2'] \subseteq \mathbb{F}$ denotes the maximum feasible frequency range where there is a feasibility for shaping the phase of the open-loop function to meet flatness constraint (10). It is seen from Fig. 9 that $\mathbb{F}'$ with $F_1' = F_1, F_2' = 334$ is obtained due to the dynamics uncertainties. Therefore, this region is the focus of the study.

Figs. 10 and 11 depict how the complementary sensitivity and sensitivity functions are expected to meet the performance metrics (10) and (11). The boundaries for the nominal and the worst-case scenarios (respectively associated with $\mathcal{M} = 1$ and the most deviation due to $\mathcal{M} \neq 1$) are calculated with regard to Remarks 6 and 7. It is seen that the bounds in the robust nonlinear control design are conserved compared to the non-robust nonlinear control design to guarantee the performance metrics for the worst-case scenario. The expected region for the case of linear control design based on the traditional loop-shaping guideline violates flatness constraint (10). Moreover, the expected regions for the sensitivity function show the possibility for improvement by nonlinear control in both the nominal and uncertain cases.

The derived regions in Fig. 9 together with Remark 8 demand for an additional control element with the constant-in-gain lead-in-phase (CgLp) property which is not realizable by linear control. Next, CgLp reset control is exploited to design the nonlinear control $\mathcal{C}$ and consequently realize the desired open-loop phase.

5.1. CgLp reset control design

CgLp reset control—introduced in Section 2— is considered as the nonlinear control $\mathcal{C}$ in Fig. 1. As it was shown in Fig. 2, it is possible to add phase to the open-loop function with almost no change in the magnitude using the first-order reset element $\mathcal{R}$ based on the 1st-order sinusoidal input describing function. The frequency response of the CgLp reset control $\mathcal{C}$ based on the 1st-order describing function is given by (4).

The reset element $\mathcal{R}$ produces higher-order harmonics in addition to the 1st harmonic. Caution is required to avoid any closed-loop stability and performance issues. Therefore, the intensity of the switching sub-dynamics $\mathcal{R}_r$ must be limited. Regarding the illustrations in Fig. 2, the closer the resetting coefficient γ to 1 and the narrower the lead band $[\omega_r, \omega_f]$, the less nonlinearity is introduced by the reset element.

Moreover, the higher-order harmonics usually cause multiple-resets at low frequency where nonlinear control is not needed because of the feedback loop. It is recalled from Section 2 that multiple-resets at a specific frequency refers to the occurrence of more than two resets per one cycle at that frequency. The describing function analysis is not valid if multiple-resets occurs, which must be avoided based on the provided

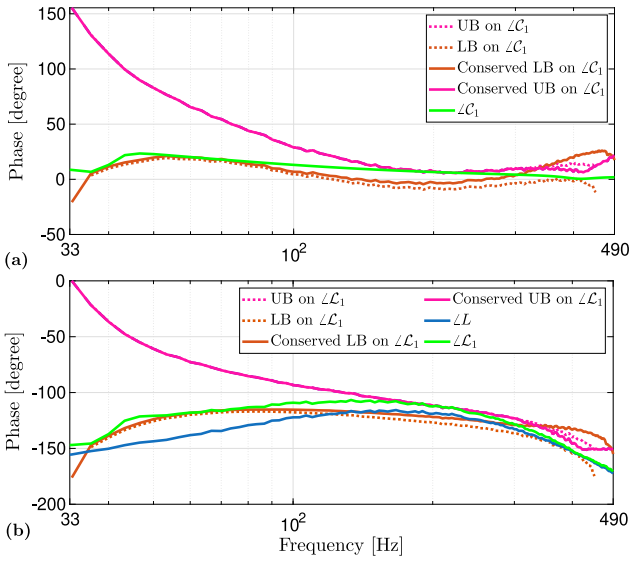

Fig. 9. The nominal and robust regions in the new loop-shaping guideline and the comparison between the open-loop functions' phases of the linear control and the nonlinear control in the critical frequency range $\mathbb{F}$; (a) The boundaries (UB: Upper bound, LB: Lower bound) of the additional required phase in addition to the CgLp phase $\angle C_1$. (b) The boundaries for shaping the open-loop function's phase on top of the open-loop functions' phases $\angle L$ and $\angle\mathcal{L}_1$ in linear and nonlinear control.

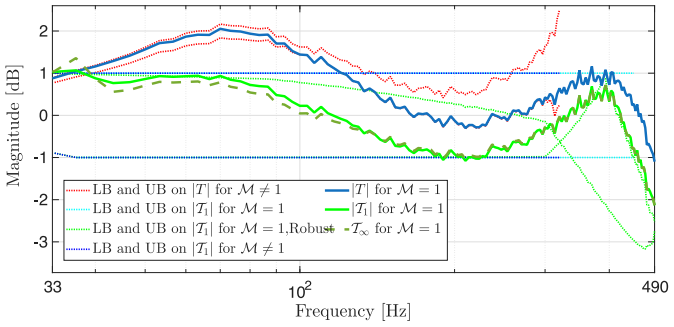

Fig. 10. The comparison of the designed nonlinear control based on the new loop-shaping guideline with the designed linear control based on the traditional guideline by the describing function-based complementary sensitivity function. In addition, the regions in nonlinear control design (dotted light blue line for non-robust design and dotted green line for robust design) and the expected regions due to the dynamics uncertainty (dotted red line for linear control and dotted dark blue line for robust nonlinear control) are specified by LB (lower bound) and UB (upper bound).

discussions in Section 2. Shaping filter, shown by C_s in Fig. 1, is a solution to avoid the multiple-resets. Next, a new simple and conceptual scheme is presented to design the shaping filter systematically.

The switching sub-dynamics $\mathcal{R}_r$ is not activated if the phase of the shaping filter is selected as $\angle C_s = \angle\mathcal{R}_{\text{bl}}$. This is intuitive based on (2) because the zero-crossing time instants are the same for e'' and $\boldsymbol{u}$, which means that there is no resetting action. In this case, the dynamics of $\mathcal{R}$ is fully described by its base linear sub-dynamics $\mathcal{R}_{\text{bl}}$ and no higher-order harmonics are generated. On the other hand, the phase advantage of $\mathcal{R}$ for the given $\gamma, \omega_r, \omega_f$ is fully available and the higher-order harmonics are not avoided if $\angle C_s = 0$ is selected. Thus, the intuitive and practical methodology for shaping filter design is given as follows:

1. Set $\angle C_s = \angle\mathcal{R}_{\text{bl}}$.
2. Specify the frequency range where reset control is needed. It is $\mathbb{F}' = [F_1', F_2']$ in the motion control design problem.

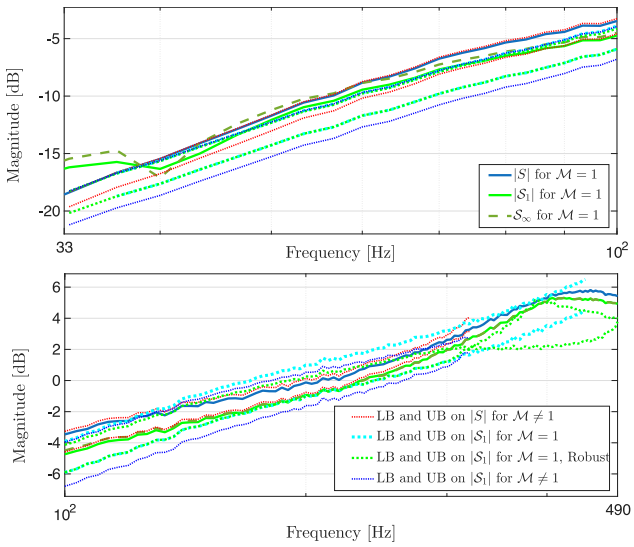

Fig. 11. The comparison of the designed nonlinear control based on the new loop-shaping guideline with the designed linear control based on the traditional guideline by the describing function-based sensitivity function. The equivalent regions in Fig. 10 are included. The figure is split in two frequency ranges for a more convenient visualization.

3. Shape $\angle C_s$ such that it is equal or greater than 0 in the frequency range $\mathbb{F}'$. For that, one notch filter around F_1', one anti-notch filter around F_2' and one lead filter are suggested.
4. Tune the parameters of the filters in the previous step to keep $\angle C_1$ within the region obtained by the new loop-shaping guideline.

The shaping filter is thus given by the following transfer function:

$$C_s(j\omega) = \frac{1}{j\frac{\omega}{\omega_r}+1}\cdot\frac{(\frac{j\omega}{\omega_N})^2+\frac{1}{Q_N\cdot\omega_N}.j\omega+1}{(\frac{j\omega}{\omega_N})^2+\frac{1}{Q'_N\cdot\omega_N}.j\omega+1}\cdot (j\frac{\omega}{\omega_h}+1).\frac{(\frac{j\omega}{\omega_A})^2+\frac{1}{Q_A\cdot\omega_A}.j\omega+1}{(\frac{j\omega}{\omega_A})^2+\frac{1}{Q'_A\cdot\omega_A}.j\omega+1} \tag{23}$$

To validate the expected performance based on the 1st-order describing function before an implementation, the difference between the 1st-order describing function-based functions $\mathcal{S}_1, \mathcal{T}_1$– where only first harmonic is considered– and pseudo functions $\mathcal{S}_\infty, \mathcal{T}_\infty$– where all the control harmonics are considered– are investigated. If the difference is not negligible, the intensity of the switching sub-dynamics is lowered.

Eventually, the parameters of the CgLp reset control including the parameters of the shaping filter are selected as in Table 1. Fig. 12 depicts the shaping filter phase $\angle C_s$ which is aligned with the presented steps for the shaping filter design. $\angle C_s$ follows $\angle R_{\text{bl}}$ before F_1. It immediately increases and decreases after F_1 and F_2 respectively.

Fig. 9(a) shows how the designed CgLp reset control realizes the additional phase requirement within most of the feasible critical frequency range $\mathbb{F}'$. As a result, the 1st-order describing function-based open-loop phase $\angle \mathcal{L}_1$ in case of the nonlinear motion control lies in almost all of the both nominal and robust regions while the open-loop phase $\angle L$ in case of the linear motion control does not satisfy the phase requirement for the nominal dynamics in $[37, 120]$ Hz and for the uncertain dynamics in $[37, 131]$ Hz, which is shown by Fig. 9(b). Thanks to the designed shaping filter, no multiple-resets occurs.

Figs. 10 and 11 show that the 1st-order describing function-based complementary sensitivity and sensitivity functions $\mathcal{T}_1, \mathcal{S}_1$ are located in the conserved bounds as long as the open-loop phase is located in the robust region except in the beginning of the frequency range of concern because the magnitude of the CgLp reset control is not perfectly

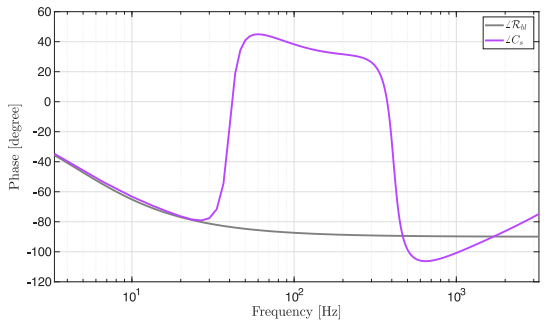

Fig. 12. The shaping filter phase together with the base linear phase.

constant. An idea is to recalculate the regions for the phase shaping by considering the slightly changed open-loop function's gain. This idea is not explored in this work to focus on the mentioned contributions. This fulfillment of the conserved bounds was expected based on the provided guarantee by Theorem 4, Corollary 5, Remarks 6 and 7. $\mathcal{S}_\infty, \mathcal{T}_\infty$ are also plotted to confirm the satisfaction of the conserved bounds by their closeness to $\mathcal{S}_1, \mathcal{T}_1$. Therefore, it is expected that the calculated dotted red and dark blue lines in Figs. 10 and 11 encounter the measured complementary sensitivity and sensitivity functions according to the provided guarantee by Theorem 4. This validation is provided in the next section by experiment.

6. Experimental results

The designed nonlinear motion control in Section 5.1 is validated and compared with the linear motion control of Section 3.2 by experiments. The laboratory setup explained in Section 3 has been used for the experiments. All of the experiments have been run around the operating point of 50 μm where the frequency response of the plant has been identified.

Fig. 13(a) depicts the measured complementary sensitivity function for the two cases of linear and nonlinear motion control. The travel range of 10 μm has been selected. The ±1 dB flatness constraint is satisfied in the frequency range of concern $\mathbb{F}'$ by nonlinear motion control–as it was expected from Theorem 4 in Section 4– while it is violated by linear motion control. Fig. 13(b) shows that the measured sensitivity function is approximately located in the region–which was calculated for the worst-case scenario– except for the beginning of $\mathbb{F}'$, which could be from the system's noise and the slight mismatch between $|S_\infty|$ and $|S_1|$ while designing the nonlinear control. This latter issue needs further considerations to be resolved in the future.

Fig. 14 depicts the triangular tracking response–a typical trajectory in precision motion systems–regarding the ±1 dB flatness constraint. 25% of the full stroke has been selected, which is the maximum considered travel range in the robust nonlinear control design. It shows that the designed nonlinear motion control is robust against the plant's nonlinearity while the linear motion control with the same cross-over frequency ω_c violates the ±1 dB bounds.

Fig. 15 depicts the achieved performance–the ±1 dB constraint–by nonlinear motion control in tracking a sinusoidal reference at 100 Hz. In contrast to the considered problem, where only 25% of uncertainty is considered, almost the full stroke operation is investigated in this experimental study. The full uncertainty in Fig. 4 makes the robust region in Fig. 9 smaller such that the open-loop phase $\angle \mathcal{L}_1$ still passes the region at 100 Hz. The ±1 dB constraint is satisfied for small and large travel ranges in the case of the nonlinear motion control while it is violated in the case of the linear motion control. The measurements presented in Fig. 14 and Fig. 15 were conducted without control redesign although the linear dynamics of the plant was probably altered due to several operations.

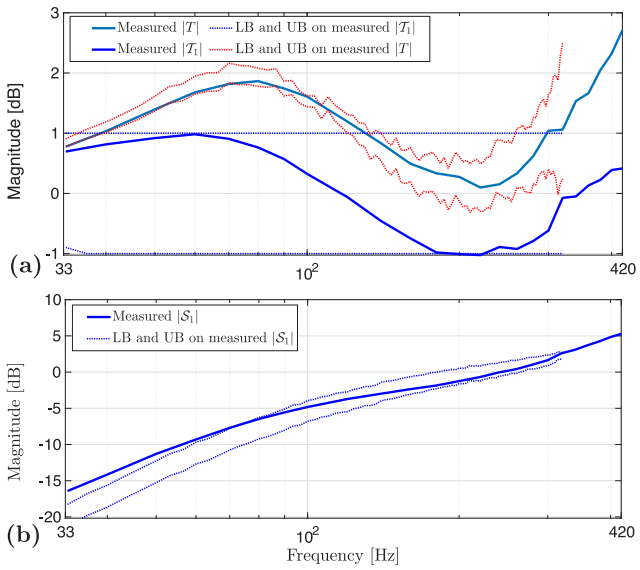

Fig. 13. Measured frequency-domain performance metrics around the operating point of 50 μm with the travel range of 10 μm–The LB (lower bound) and UB (upper bound) specify the expected region for the nonlinear dynamics; (a) Describing function-based complementary sensitivity function $|\mathcal{T}_1|$. (b) Describing function-based sensitivity function $|\mathcal{S}_1|$.

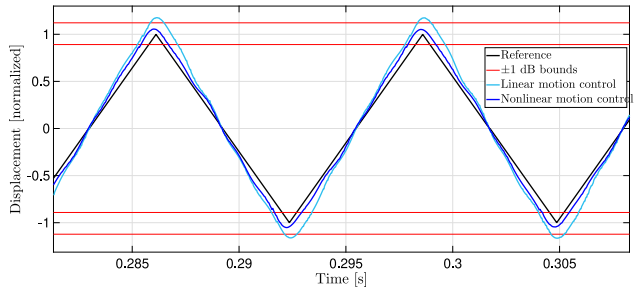

Fig. 14. Triangle reference tracking at 80 Hz.

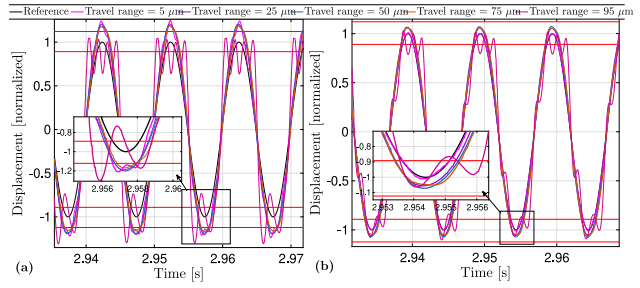

Fig. 15. Sinusoidal tracking for different travel ranges where the red lines specify the ±1 dB constraint; (a) Linear motion control. (b) Nonlinear motion control. It is noted that the phase shifts are not shown.

The cumulative power spectral density of the sinusoidal tracking errors in linear and nonlinear motion control are shown in Fig. 16 for different travel ranges. Additionally, the boundaries for the nonlinear dynamics in Fig. 11 have been converted to the boundaries on the power spectral density and are shown here. The plots are devided by the input's power and then multiplied by 2 for normalization.

By selecting the normal structure of CgLp (see e.g., [29]), it is simply possible to shape the open-loop phase $\angle\mathcal{L}_1$ following the designed steps for the shaping filter design. Therefore, it is easy to guide the CgLp

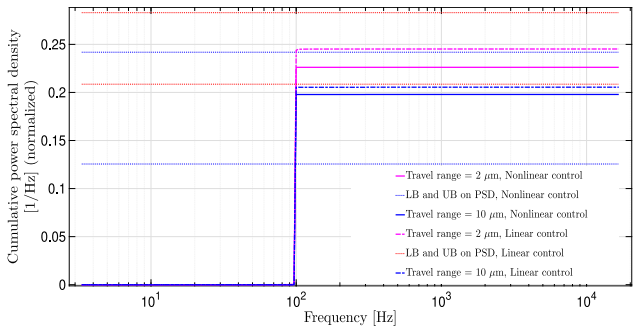

Fig. 16. The comparison of the designed nonlinear motion control with the designed linear motion control by the cumulative power spectral density of the error in sinusoidal tracking at 100 Hz. The pre-calculated LB (lower bound) and UB (upper bound) on PSD (power spectral density) are indicated for both linear and nonlinear control.

reset control phase completely through the robust region. In addition, the slight change in the gain of the CgLp reset control with normal structure is in favor of the sensitivity function, unlike the considered structure in this work. However, this approach needs an aggressive resetting sub-dynamics $\mathcal{R}_r$, which leaves the 1st-harmonic analysis unreliable. This is our future research direction to let implement a highly aggressive reset control with reliable 1st-order sinusoidal input describing function-based control design.

7. Conclusion

It was shown that the open-loop phase is crucial for performance within a wide range of frequency for motion control design of piezo-actuated positioners. A new set of guidelines for loop shaping was presented by rigorous analytical formulations. The guidelines were extended to the case with dynamics uncertainty due to the nonlinearities of the large travel ranges. An effective reset control design was provided by presenting a practical and intuitive methodology for shaping filter design.

A rigorous analysis of closed-loop convergence would further strengthen the reliability of the proposed reset control framework, particularly for broader applications in piezo-positioning systems. The extension of the guidelines to reset control design by loop shaping for systematic integration with the state-of-the-art hysteresis compensator, inner-loop active damping control, and feedforward control represents a meaningful direction for future research. In addition, the development of more aggressive CgLp reset control strategies aimed at achieving substantial performance improvements– where shaping filters alone may be insufficient for a successful realization of loop shaping– is considered an interesting direction for further research.

CRediT authorship contribution statement

A. Sebghati: Writing – review & editing, Writing – original draft, Visualization, Validation, Software, Methodology, Investigation, Formal analysis, Conceptualization. **S.H. HosseinNia:** Writing – review & editing, Supervision.

Declaration of Generative AI and AI-Assisted Technologies in the Writing Process

During the preparation of this work the author(s) used ChatGPT in order to improve the writing style. After using this tool/service, the author(s) reviewed and edited the content as needed and take(s) full responsibility for the content of the publication.

Declaration of competing interest

The authors declare the following financial interests/personal relationships which may be considered as potential competing interests: Ashkan Sebghati reports financial support was provided by Physik Instrumente (PI) GmbH & Co KG. S. Hassan HosseinNia reports financial support was provided by Physik Instrumente (PI) GmbH & Co KG. If there are other authors, they declare that they have no known competing financial interests or personal relationships that could have appeared to influence the work reported in this paper.

Acknowledgments

This work was financed by Physik Instrumente (PI) SE & Co. KG and co-financed by Holland High Tech with PPS Project supplement for research and development in the field of High Tech Systems and Materials.

The authors express their sincere gratitude to both Mathias Winter, Head of Piezo System & Drive Technology, and Dr.-Ing. Simon Kapelke, Head of Piezo Fundamental Technology, from Physik Instrumente (PI) SE & Co. KG, for their invaluable collaboration in providing technical insights concerning the system and its applications.

Data availability

Data will be made available on request.

References

[1] Schmidt RM, Schitter G, Rankers A. The design of high performance mechatronics-: high-Tech functionality by multidisciplinary system integration. Ios Press; 2020.
[2] Ru C, Liu X, Sun Y, et al. Nanopositioning technologies. Fundam Appl 2016.
[3] Clegg JC. A nonlinear integrator for servomechanisms. Trans Am Inst Electr Eng Part II: Appl Ind 1958;77(1):41–2.
[4] Heertjes M, van Den Eijnden S, Sharif B. An overview on hybrid integrator-gain systems with applications to wafer scanners. In: 2023 IEEE international conference on mechatronics. IEEE; 2023, p. 1–8.
[5] Beker O, Hollot CV, Chait Y. Plant with integrator: an example of reset control overcoming limitations of linear feedback. IEEE Trans Autom Control 2002;46(11):1797–9.
[6] Heertjes M, Gruntjens K, Van Loon S, Van de Wouw N, Heemels W. Experimental evaluation of reset control for improved stage performance. IFAC-PapersOnLine 2016;49(13):93–8.
[7] Zhao G, Nešić D, Tan Y, Hua C. Overcoming overshoot performance limitations of linear systems with reset control. Automatica 2019;101:27–35.
[8] Saikumar N, Heinen K, HosseinNia SH. Loop-shaping for reset control systems: A higher-order sinusoidal-input describing functions approach. Control Eng Pract 2021;111:104808.
[9] Zhao G, Nešić D, Tan Y, Wang J. Open problems in reset control. In: 52nd IEEE conference on decision and control. IEEE; 2013, p. 3326–31.
[10] Zhang X, HosseinNia SH. Identifying two-reset conditions for closed-loop sinusoidal input reset control systems. In: 2024 20th IEEE/aSME international conference on mechatronic and embedded systems and applications. IEEE; 2024, p. 1–6.
[11] Karbasizadeh N, Dastjerdi AA, Saikumar N, HosseinNia SH. Band-passing nonlinearity in reset elements. IEEE Trans Control Syst Technol 2022;31(1):333–43.
[12] Zhang X, HosseinNia SH. Enhancing the reliability of closed-loop describing function analysis for reset control applied to precision motion systems. 2024, arXiv preprint arXiv:2412.00502.
[13] Zhong J, Yao B. Adaptive robust precision motion control of a piezoelectric positioning stage. IEEE Trans Control Syst Technol 2008;16(5):1039–46.
[14] Sabarianand D, Karthikeyan P, Muthuramalingam T. A review on control strategies for compensation of hysteresis and creep on piezoelectric actuators based micro systems. Mech Syst Signal Process 2020;140:106634.
[15] Esbrook A, Tan X, Khalil HK. Control of systems with hysteresis via servocompensation and its application to nanopositioning. IEEE Trans Control Syst Technol 2012;21(3):725–38.
[16] Nuij PWJM. Higher order sinusoidal input describing functions: extending linear techniques towards non-linear systems analysis [Ph.D. thesis], Technische Universiteit Eindhoven; 2007.
[17] Alferink D, Fey RH, Van De Wouw N, Heertjes MF. Hysteresis in motion control systems: a frequency-domain analysis on higher harmonics. In: 2025 American control conference. IEEE; 2025, p. 5073–8.
[18] Guo Y, Wang Y, Xie L. Frequency-domain properties of reset systems with application in hard-disk-drive systems. IEEE Trans Control Syst Technol 2009;17(6):1446–53.
[19] Hou X, Dastjerdi AA, Saikumar N, Hosseinnia SH. Tuning of 'constant in gain lead in phase (CgLp)'reset controller using higher-order sinusoidal input describing function (HOSIDF). In: 2020 Australian and New Zealand control conference. IEEE; 2020, p. 91–6.
[20] Zhang X, HosseinNia SH. Enhancing reset control phase with lead shaping filters: Applications to precision motion systems. 2025, arXiv preprint arXiv:2503.15020.
[21] Hosseini SA, Quinten FR, van Eijk LF, Kostic D, HosseinNia SH. Frequency domain design of a reset-based filter: An add-on nonlinear filter for industrial motion control. 2025, arXiv preprint arXiv:2507.01491.
[22] Dastjerdi AA, Astolfi A, Saikumar N, Karbasizadeh N, Valerio D, HosseinNia SH. Closed-loop frequency analysis of reset control systems. IEEE Trans Autom Control 2022;68(2):1146–53.
[23] Beker O, Hollot C, Chait Y, Han H. Fundamental properties of reset control systems. Automatica 2004;40(6):905–15.
[24] Carrasco J, Baños A, Barreiro A. Stability of reset control systems with inputs. In: 2008 16th mediterranean conference on control and automation. IEEE; 2008, p. 1496–501.
[25] Baños A, Carrasco J, Barreiro A. Reset times-dependent stability of reset control systems. IEEE Trans Autom Control 2010;56(1):217–23.
[26] Dastjerdi AA, Astolfi A, HosseinNia SH. Frequency-domain stability methods for reset control systems. Automatica 2023;148:110737.
[27] Van Loon S, Gruntjens K, Heertjes MF, van de Wouw N, Heemels W. Frequency-domain tools for stability analysis of reset control systems. Automatica 2017;82:101–8.
[28] Guo Y, Gui W, Yang C, Xie L. Stability analysis and design of reset control systems with discrete-time triggering conditions. Automatica 2012;48(3):528–35.
[29] Sebghati A, HosseinNia SH. Robust reset control design for piezo-actuated nanopositioner in presence of hysteresis nonlinearity. 2025, arXiv preprint arXiv:2510.09445.